ACSNANO

www.acsnano.org

ARTICLE

Full-Color Light-Emitting Carbon Dots with a Surface-State-Controlled Luminescence Mechanism

Hui Ding, Shang-Bo Yu, Ji-Shi Wei, and Huan-Ming Xiong*

Department of Chemistry, Fudan University, Shanghai 200433, P. R. China

Supporting Information

ABSTRACT: Carbon dots (CDs) with tunable photoluminescence (PL) and a quantum yield of up to 35% in water were hydrothermally synthesized in one pot and separated *via* silica column chromatography. These separated CDs emitted bright and stable luminescence in gradient colors from blue to red under a single-wavelength UV light. They exhibited high optical uniformity; that is, every sample showed only one peak in the PL excitation spectrum, only one peak in the excitation-independent PL emission spectrum, and similar monoexponential fluorescence lifetimes. Although these samples had similar distributions of particle size and graphite structure in their carbon cores, the surface state gradually varied among the samples, especially the degree of oxidation. Therefore, the observed red shift in their emission peaks from 440 to 625 nm was ascribed to a gradual reduction in their band gaps with the increasing incorporation of oxygen species into their surface structures. These energy bands were found to depend on the surface groups and structures but not on the particle size, not as in traditional semiconductor quantum dots. In addition, because of their excellent PL properties and low cytotoxicity, these CDs could be used to image cells in different colors under a single-wavelength light source, and the red-emitting CDs could be used to image live mice because of the strong penetration capability of their fluorescence.

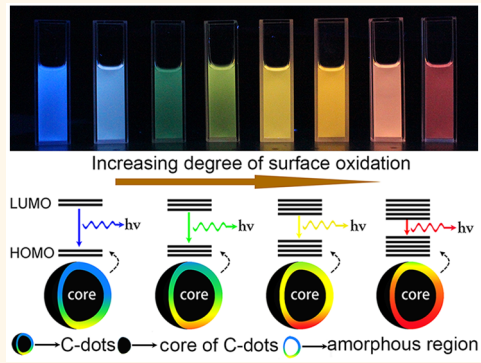

KEYWORDS: *carbon dots, full-color luminescence, luminescence mechanism, surface states, bioimaging*

Because of their outstanding merits in terms of luminescence, stability, biocompatibility, and low cost, carbon dots (CDs) have been intensively studied over the past decade for potential applications in fluorescent probes, light-emitting devices, and biosensors.[1−3] Thousands of raw materials and hundreds of approaches have been reported for the synthesis of CDs. The reported raw materials vary from laboratory-produced chemicals to natural products, whereas the approaches include laser ablation, pyrolysis, electrochemical oxidation, hydrothermal reactions, and microwave treatment.[4−6] In most studies, the photoluminescence (PL) emission spectra of such CDs have been broad, with maxima in the blue region, and their absorption curves have shown gradual attenuation without significant absorption bands,[7−10] implying that conventional CDs are produced in complex mixtures and that a complete isolation of products is strongly desired. Several separation techniques have been reported for this purpose that offer high separation efficiency, such as high-performance liquid chromatography (HPLC)[11−15] and polyacrylamide gel electrophoresis (PAGE).[16] However, only tiny amounts of products can be obtained using these techniques, which limits their further application. In addition, conventional CDs cannot be effectively used to image animals because of their low quantum yield (QY) in both the red and near-infrared regions.[17,18] Underlying the great difficulty encountered in controlling CD fluorescence is the fact that the luminescence mechanisms of CDs remain unclear.[19,20] Because CDs are prepared using numerous ingredients and various approaches and contain multiple complicated components and structures, it is extremely difficult to compare the results available in the literature to formulate a unified theory.[21−23] Therefore, a study of the tuning of CD fluorescence under controlled, comparable conditions would be beneficial for determining the luminescence mechanisms of CDs and, consequently, for obtaining CDs with strong red emission.

To date, there have been only a few successful reports of CDs with tunable PL from blue to red. For example, Hu *et al.* produced a series of CDs by varying the reagents and concluded that epoxides or hydroxys on their surfaces were predominantly responsible for the resulting PL red shift.[19] Lin *et al.* synthesized three types of CDs with blue, green, and red

Received: August 28, 2015
Accepted: December 5, 2015
Published: December 8, 2015

DOI: 10.1021/acsnano.5b05406
ACS Nano 2016, 10, 484−491

emission by solvothermally treating different carbon sources and ascribed the observed PL red shift to quantum size effects and the nitrogen content of the CDs.[24] Pang and colleagues prepared a series of CDs by modifying the reaction conditions and ascribed the PL red shift to both quantum size effects and surface states.[25] Although CDs with tunable PL have been successfully obtained, the conclusions regarding the corresponding mechanisms are controversial and even contradictory. When different samples with complex compositions were studied together, the derived PL mechanisms were not convincing because there were too many factors influencing the luminescence processes, particularly the different synthesis conditions used.[26−29] Furthermore, most reported red-emitting CDs have suffered from QYs of less than 5% in water, thereby limiting their further application in animal imaging.

Herein, we report the first one-pot syntheses of full-color light-emitting CDs. The QY of the red-emitting CDs is approximately 24%, as accurately measured using an integration sphere, which is the highest value yet recorded for CDs in water. The fully purified CDs exhibit excitation-independent luminescence from blue to red, characterized by a single excitation peak and a monoexponential lifetime. Their PL red shift shows a direct relationship with the degree of surface oxidation of the CDs, excluding quantum size effects; on the basis of this finding, we propose a reasonable PL mechanism. Our CDs can be successfully applied for bioimaging, both *in vitro* and *in vivo*, by virtue of their high QY, stable PL, and low toxicity.

RESULTS AND DISCUSSION

Many reagents were experimentally tested in pairs under hydrothermal conditions, and the products were observed under UV light to judge whether they merited further investigation. In most cases, the as-prepared solutions emitted blue-green fluorescence (Figure S1). Urea and *p*-phenylenediamine were ultimately selected because their products yielded yellow-red fluorescence, indicating that red-emitting CDs were dominant. Afterward, the mass ratio between urea and *p*-phenylenediamine was adjusted in parallel reactions, and a ratio of 1:1 was found to be optimal for the strongest fluorescence (Figure S2). Similarly, the optimal temperature and reaction time were determined to be 160 °C and 10 h, respectively (Figure S3). The as-prepared products were actually mixtures of CDs with different colors of fluorescence, which could be critically separated *via* silica column chromatography because they had different polarities. Interestingly, the quantitative ranking of their polarities precisely coincided with their ordering in terms of a gradual color change from blue to red. Finally, eight samples with distinct fluorescence characteristics were successfully collected and found to exhibit a gradient of colors under a single-wavelength UV light (Scheme 1). It should be noted that the operation of the silica column chromatography apparatus required great patience and attentiveness. Complete fractionation required more than 10 h because it was necessary to maintain a slow flow rate to avoid cross-contamination of different CDs, whereas the polarity of the eluting solvents needed to be gradually increased for each fraction throughout the entire process. The obtained CDs were separately freeze-dried and dispersed in water for use. Four typical samples exhibiting blue, green, yellow, and red fluorescence were selected for further characterization; these samples were labeled as samples A, B, C and D, respectively.

Scheme 1[a]

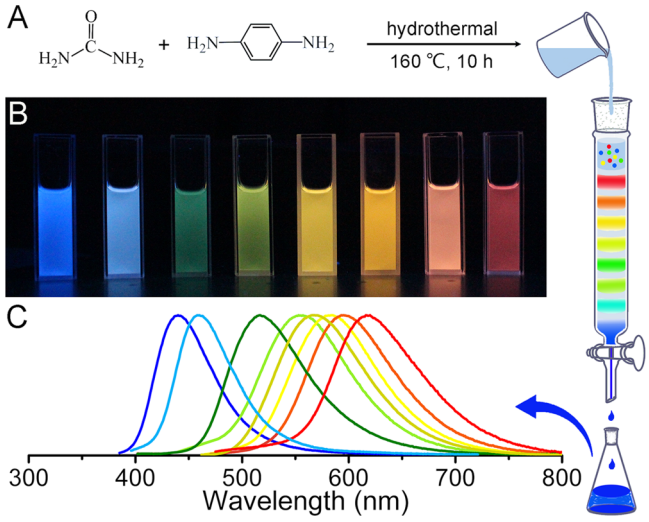

[a](A) One-pot synthesis and purification route for CDs with distinct fluorescence characteristics. (B) Eight CD samples under 365 nm UV light. (C) Corresponding PL emission spectra of the eight samples, with maxima at 440, 458, 517, 553, 566, 580, 594, and 625 nm.

The UV−vis absorption spectra of the four selected samples, as shown in Figure 1, display analogous absorption in the UV region of 200−350 nm but different behaviors in the lower-energy region. In the UV region of each curve, a single peak is observed at 255 nm with a shoulder at 282 nm, corresponding to the $\pi-\pi^*$ transitions of C═C and C═N bonds, respectively, in the aromatic rings, which do not typically

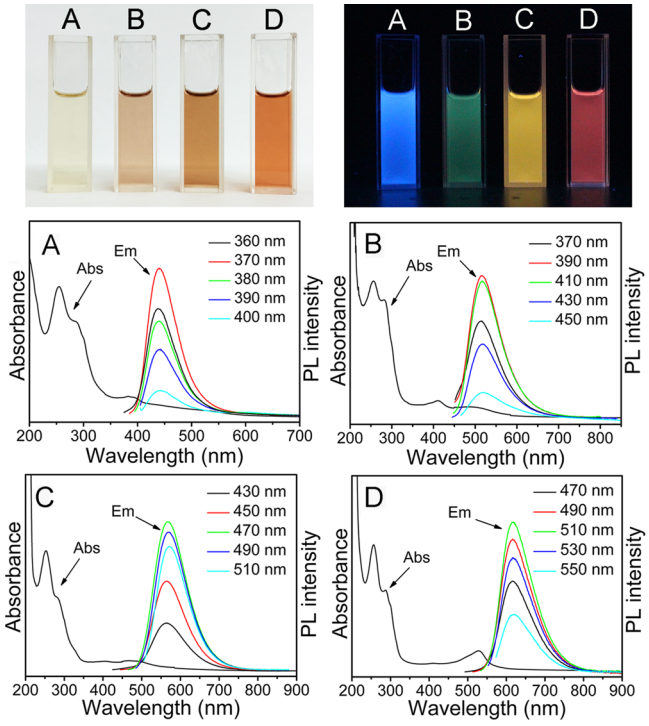

Figure 1. Top images are photographs of samples A, B, C, and D in aqueous solution under daylight (left) and UV light (right). The bottom four graphs show their absorption curves (Abs) and their PL emission spectra (Em) under excitation with light of different wavelengths (see the inset legends).

DOI: 10.1021/acsnano.5b05406
ACS Nano 2016, 10, 484−491

generate fluorescence.[30−32] However, in the lower-energy region, the four spectra exhibit distinct absorption bands at 383, 410, 488, and 528 nm, indicating that these samples possessed different surface states.[22,33] Unlike many other reported CDs,[34,35] the PL emission peaks of our samples did not shift when different excitation wavelengths were applied. Moreover, the corresponding PL excitation curve of each sample was found to have only one peak (Figure S4), with a position quite close to that of the absorption band in the lower-energy region. These results confirm the uniformity of our samples in terms of their optical features; that is, the CDs in each sample had identical absorption structures and luminescent centers. The PL emission of each sample clearly originated from the absorption in the lower-energy region. Furthermore, the time-resolved photoluminescence (TRPL) spectra of these samples were measured, and the results indicated similar monoexponential lifetimes of approximately 9 ns, implying that all of the CDs underwent similar luminescence processes (Figure S5 and Table S4).[36] The optical uniformity of these samples facilitated a deep investigation of their luminescence mechanisms based on a comparison of their compositions and structures.

The transmission electron microscopy (TEM) images presented in Figure 2 reveal that the samples were well-

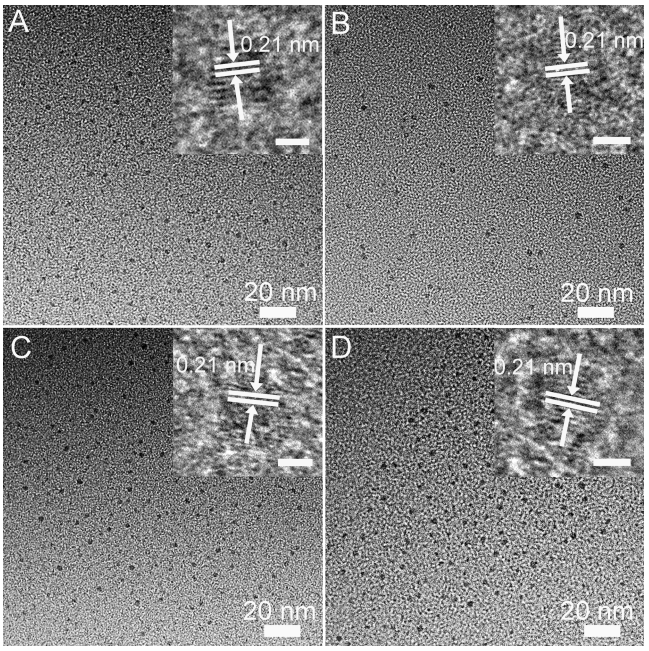

Figure 2. TEM and HRTEM (inset) images of the four selected samples. The scale bars in the insets represent 2 nm.

dispersed, with similar average particle sizes of approximately 2.6 nm (Figure S6). The high-resolution (HR) TEM images provided in the insets show that all of the CDs exhibited identical well-resolved lattice fringes with a spacing of 0.21 nm, corresponding to the (100) in-plane lattice of graphene.[37] Interestingly, after critical separation, the particle size distributions of these samples remained so broad that their differences in fluorescence cannot be obviously ascribed to differences in particle size. The TEM data clearly demonstrate that the PL emission red shift of the samples from A to D is not due to quantum size effects. The Raman spectra of these CDs (Figure S7) reveal a D band at 1352 cm^{-1} and a G band at 1595 cm^{-1}, which correspond to disordered structures and graphitic structures, respectively, of carbon materials.[38−40] The intensity ratio I_D/I_G was found to increase from 0.87 to 1.13 for sample A to sample D, suggesting that the amorphous structures of the CDs were closely related to the red shift of the PL emission.

The Fourier transform infrared (FTIR) spectra shown in Figure 3 reveal that all CD samples possessed abundant

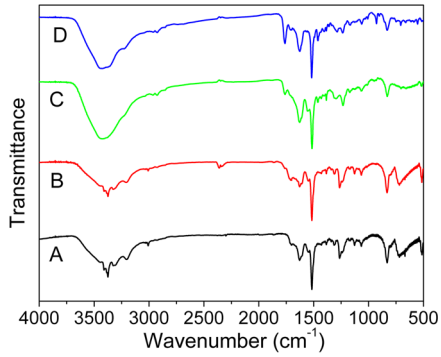

Figure 3. FTIR spectra of the four selected CD samples.

hydrophilic groups such as O−H (3425 cm^{-1}), N−H (3200 cm^{-1}), C−O (1258 cm^{-1}), and COOH (1759 cm^{-1}) on their surfaces, thereby ensuring their good solubility in water.[41] Moreover, stretching vibrations of C═C (1524 cm^{-1}), C═N (1642 cm^{-1}), and C−N= (1427 cm^{-1}) bonds were observed for each sample, indicating the formation of polyaromatic structures in the CDs during the reaction process.[42,43] A comparison of the FTIR spectra of the four samples reveals two important observations. One is an enhancement of the typical stretching vibration of COOH bonds at 1759 cm^{-1} from sample A to sample D, indicating an increase in the degree of oxidation accompanying the PL red shift of the CDs.[33] The other is that the O−H vibration bands at approximately 3420 cm^{-1} are sharp and discrete for samples A and B but broad and integrated for samples C and D. In general, a broad O−H band indicates multiple structures of hydroxyl groups on the nanoparticle surfaces, resulting in higher polarity and hydrophilicity of samples C and D compared with samples A and B.[44]

X-ray photoelectron spectroscopy (XPS) findings were used to further investigate the surfaces of these samples. The full spectra presented in Figure S8 show three typical peaks: C 1s (285 eV), N 1s (400 eV), and O 1s (531 eV). These findings indicate that the samples consisted of the same elements.[45] In the high-resolution spectra (Figure 4), the C 1s band can be deconvoluted into four peaks, corresponding to sp^2 carbons (C═C, 284.5 eV), sp^3 carbons (C−O/C−N, 286.1 eV), carbonyl carbons (C═O, 287.8 eV), and carboxyl carbons (COOH, 289.0 eV).[46] The N 1s band can be deconvoluted into three peaks at 398.4, 399.1, and 400.2 eV, representing pyridinic N, amino N, and pyrrolic N, respectively. The O 1s band contains two peaks at 531.6 and at 533.0 eV for C═O and C−O, respectively.[24,26] The XPS intensity at 289.0 eV gradually increases from sample A to sample D, implying a corresponding increase in the content of carboxyl groups in the CDs (Table 1), consistent with the FTIR results. The atomic ratio between oxygen and carbon increases from 0.05 to 0.21 as the O content increases from 6.00 to 20.20% for sample A to sample D (Tables S5 and S6), reflecting the same tendency in the degree of oxidation enhancement of the CDs. The above data, including the Raman, FTIR, and XPS results, clearly

DOI: 10.1021/acsnano.5b05406
ACS Nano 2016, 10, 484−491

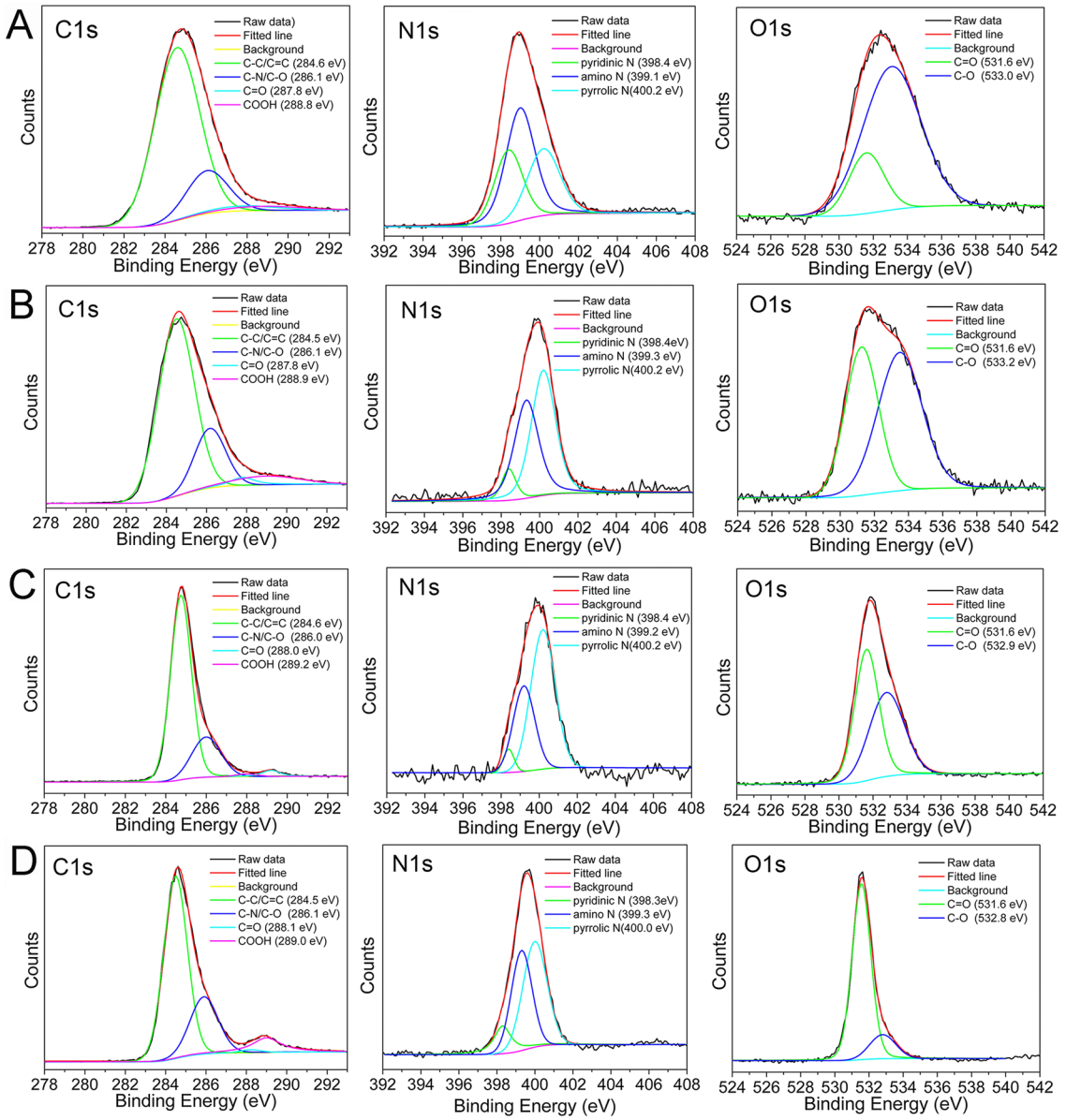

Figure 4. High-resolution XPS C 1s, N 1s, and O 1s spectra of the four selected samples. Each band was deconvoluted following the literature.

Table 1. XPS Data Analyses of the C 1s Spectra of Four Typical CD Samples

sample	C═C/C−C	C−N/C-O	C═O	COOH
A	76.19%	17.52%	3.21%	3.08%
B	73.76%	19.12%	2.88%	4.24%
C	70.11%	21.07%	2.45%	6.37%
D	67.05%	21.75%	2.90%	9.30%

exhibit that our CDs consisted of π-conjugated domains in their carbon cores and amorphous regions on their surfaces and that the degree of oxidation of these CDs increased concurrently with the PL red shift.

Although the PL mechanisms for CDs remain unclear, the amazing PL of CDs continues to motivate scientists to conduct deeper explorations. Two popular PL models have been proposed for CDs: one is based on the band gap transitions in conjugated π-domains, and the other is related to surface defects on the CDs.[29,47−49] In accordance with the former mechanism, several reports ascribed the PL red shift of CDs to quantum size effects.[24,25] However, in our case, we believe surface states to be the dominant factor controlling the PL variations because all of our samples exhibited similar particle sizes with broad size distributions. Meanwhile, structural characterizations confirmed that both the carboxyl contents and oxidation degrees of the CD surfaces increased with the red shift of the PL. It has been reported that surface defects, which are primarily created through surface oxidation, serve as capture centers for excitons, thus giving rise to surface-state-related fluorescence.[25] A higher degree of oxidation on the CD surfaces implies more surface defects.[33] Another report by Chen *et al.* has noted that the carboxyl groups on sp^2-hybridized carbons could induce significant local distortions, resulting in a narrower energy gap; this finding was based on density functional theory.[50] In the present work, the fluorescence can undoubtedly be attributed to the surfaces of the CDs, and the surface states control the PL features. Because the PL features of our CDs behave similarly to certain types of molecular fluorescence,[51] we hypothesize that the luminescent centers on

DOI: 10.1021/acsnano.5b05406
ACS Nano 2016, 10, 484−491

the CD surfaces are predominantly composed of conjugated carbon atoms and bonded oxygen atoms. The band gap of such a structure between the highest occupied molecular orbital (HOMO) and the lowest unoccupied molecular orbital (LUMO) strongly depends on the incorporated oxygen species.[19] The band gap is reduced as an increasing number of oxygen atoms join the structure; that is, a PL red shift arises as a result of the increase in the degree of surface oxidation (Figure 5). To further confirm that the tunable PL originated

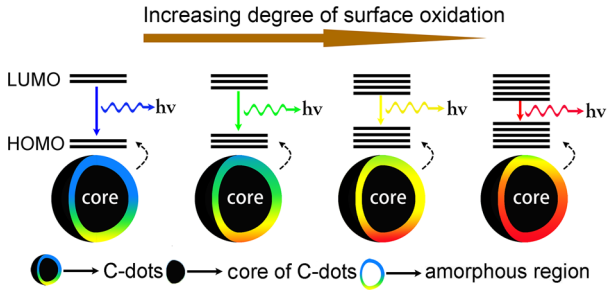

Figure 5. Model for the tunable PL of CDs with different degrees of oxidation.

from the surface states, the pH-dependent behavior of the red-emitting CDs was investigated. In Figure S9, the red emission of the CDs is shown to decay in both acidic and basic environments, and the PL peak significantly red shifts as the pH value decreases. These results may be attributed to changes in the surface charge induced by protonation−deprotonation, similar to the observed performance of other carboxyl-grafted carbon dots in the literature.[30,52−54] It should be noted that the photoluminescence intensities for pH values of 5−11 exhibited no obvious decay, which is beneficial for practical applications in *in vivo* environments.[55]

Before the application of our CDs as fluorescent probes, the luminescence stability of these CDs was tested using a UV lamp of 500 W under 1 h of irradiation, and almost no PL attenuation was observed (Figure S10). Then, standard MTT (3-(4,5-dimethylthiazol-2-yl)-2,5-diphenyltetrazolium bromide) assays were conducted using HeLa cells, revealing that these CDs are effectively nontoxic at concentrations of up to 200 μg/mL (Figure S11).[56] This high PL stability and low cytotoxicity confirm the suitability of these CDs for bioimaging applications. Figure 6 shows that after incubation at a CD concentration of 40 μg/mL for 2 h, the HeLa cells emitted strong blue, green, yellow, and red fluorescence, predominantly in the cytoplasm, under illumination at a single wavelength of 405 nm. In addition to *in vitro* cell imaging, *in vivo* mouse imaging was tested using sample D. Figure 7A shows the clear fluorescence observed in a nude mouse that was subcutaneously injected with 100 μL of sample D solution (175 μg/μL). To obtain Figure 7B, the same dosage of sample D was intravenously injected into a nude mouse through the tail vein, and after 30 min of circulation, strong fluorescence was observed in the bladder, indicating that the CDs could be rapidly excreted *via* urination.[57] The mice experiments were successfully performed using a Bruker *in vivo* imaging system with 510 nm excitation light and a 700 nm emission filter, thereby confirming that the red PL of sample D could efficiently penetrate mouse skin and tissues. Furthermore, all mice remained healthy after the injections, demonstrating the excellent biocompatibility of our CDs.

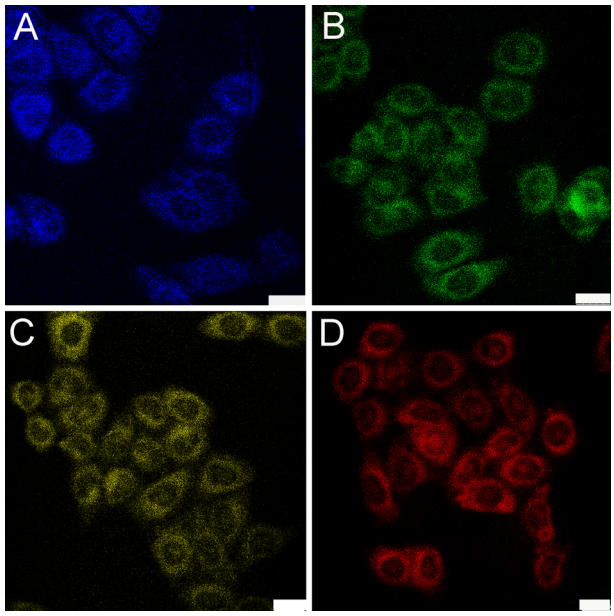

Figure 6. Confocal fluorescence images of HeLa cells incubated with 40 μg/mL of samples A, B, C, and D for 2 h. All images were obtained under excitation at 405 nm, but the emissions were recorded in different ranges: (A) 420−510 nm, (B) 490−560 nm, (C) 540−590 nm, and (D) 590−750 nm. Each scale bar represents 25 μm.

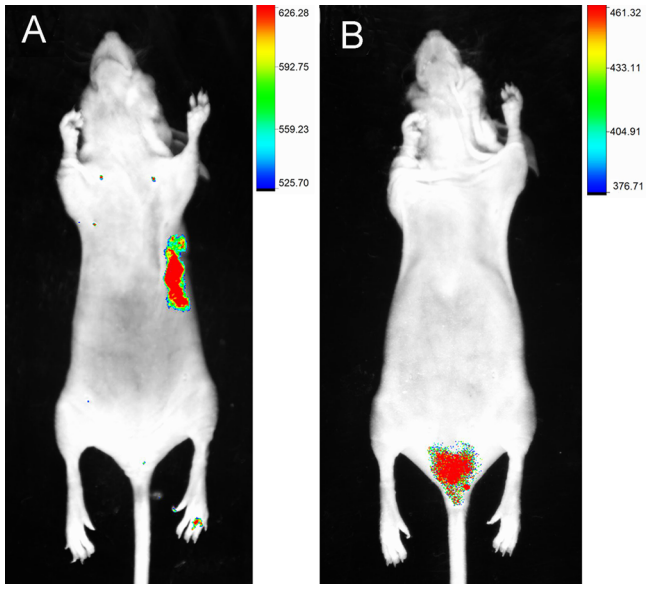

Figure 7. *In vivo* fluorescence images of nude mice treated with (A) subcutaneous injection and (B) intravenous injection of 100 μL of an aqueous solution of red-emitting CDs. The color bars represent the fluorescence intensity.

CONCLUSION

We report a facile approach to the preparation of CDs in water with full-color emission that is independent of the excitation wavelength and the successful application of samples prepared in this manner for bioimaging, both *in vitro* and *in vivo*. The key step of preparation was the critical separation of the CDs *via* column chromatography following the hydrothermal treatment of carefully selected raw materials, which was also beneficial for exploring the PL mechanisms of CDs because the samples

DOI: 10.1021/acsnano.5b05406
ACS Nano 2016, 10, 484−491

differed only with regard to their surface states. Detailed characterizations proved that different surface states of the CD samples resulted from different degrees of oxidation on their surfaces, ultimately determining the colors of their PL. We propose a new model of the PL mechanism for CDs, which suggests a method of controlling the PL features of CDs through the incorporation of heteroatoms. The full-color light-emitting CDs with high photostability and biocompatibility that are prepared in this manner, particularly those with strong red fluorescence, have promising applications in multicolor displays and biomedical probes.

METHODS

Chemicals. Urea, *p*-phenylenediamine, ethyl acetate, and ethanol were obtained from Sinopharm Chemical Reagent Co. (China). Dulbecco's modified Eagle's medium (DMEM, High Glucose), fetal bovine serum (FBS), and trypsinase were acquired from Gibco BRL (USA), and 3-(4,5-dimethylthiazol-2-yl)-2,5-diphenyltetrazolium bromide (MTT) was obtained from Sigma-Aldrich. All chemicals were used as received. Ultrapure water (Milli-Q water) was used in all experiments.

Synthesis of CDs. First, 0.2 g of urea and 0.2 g of *p*-phenylenediamine were dissolved in 50 mL of water; then, the solution was transferred into a poly(*para*-phenol)-lined stainless steel autoclave. After being heated at 160 °C for 10 h and then cooled to room temperature, the obtained solution was purified *via* silica column chromatography using a mixture of ethyl acetate and ethanol as the eluent. Afterward, the obtained CD samples with different fluorescence were redispersed in water. The detailed characterizations and bioimaging experiments that were performed are described in the Supporting Information.

MTT Assays. HeLa cells were seeded into a 96-well cell culture plate in DMEM at a density of 5×10^4 cells/mL with 10% FBS and 5% CO_2 and incubated at 37 °C for 24 h. Afterward, the culture medium was replaced with 200 μL of DMEM containing different doses of CDs, and the cells were cultured for another 48 h. Then, 20 μL of 5 mg/mL MTT solution was added to each well. The cells were incubated for a further 4 h, followed by the removal of the culture medium with MTT; 150 μL of DMSO was then added to each well. The resulting mixture was shaken for 15 min at room temperature. The absorbance of MTT at 492 nm was measured using an automatic ELISA analyzer (SPR-960). Control experiments without CDs were also performed. Each experiment was conducted five times, and the data were averaged.

Cell Imaging. Cellular fluorescence images were recorded using a Leica TCS SP5 laser scanning confocal microscope. HeLa cells were seeded into 6-well culture plates at a density of 10^5 per well in DMEM containing 10% FBS and incubated at 37 °C in a 5% CO_2 incubator for 24 h. After the removal of the DMEM, a mixture of CDs (40 μg/mL) in DMEM was added to each well for 2 h of incubation. Finally, the cells were washed twice with phosphate buffer solution to remove extracellular CDs and subsequently fixed with 4% paraformaldehyde.

QY Measurements. The quantum yield was tested using an F-3018 quantum yield accessory, which included an integrating sphere that was attached to a Horiba Jobin Yvon FluoroMax-4 spectrofluorometer. First, an aqueous solution of blue-emitting CDs was diluted to an absorption intensity of below 0.1 at the optimal excitation wavelength of 371 nm. Subsequently, this aqueous solution was added to a 10 mm fluorescence cuvette, placed in the integrating sphere and excited with monochromatic light at 371 nm. The fluorescence spectra were recorded in the ranges of 361–381 and 386–720 nm. The fluorescence spectra of pure water were also recorded under identical conditions. Finally, fluorescence software was used to calculate the QYs based on the spectra of both the sample and the water. Each experiment was performed three times in parallel to obtain the average QY value. Moreover, the QYs of the other CD samples were measured using similar procedures, differing only in the optimal excitation wavelengths and the ranges in which the PL emission was recorded (Table S2).

Characterizations. A JEM-2010 transmission electron microscope operating at 200 kV was used to obtain high-resolution transmission electron microscopy images. The UV–vis absorption spectra were measured on a Unico UV-2802 PC spectrometer. The fluorescence spectra were recorded using a Horiba Jobin Yvon FluoroMax-4 spectrofluorometer. The FTIR spectra were recorded on a Nicolet Nexus 470 FTIR spectrometer. The Raman spectra were recorded using an XploRA Raman spectrometer at an excitation wavelength of 785 nm. The X-ray photoelectron spectra were recorded using an AXIS Ultra DLD spectrometer. Time-resolved fluorospectroscopy was performed using an FLS 920 spectrometer.

ASSOCIATED CONTENT

Supporting Information

The Supporting Information is available free of charge on the ACS Publications website at DOI: 10.1021/acsnano.5b05406.

Optical properties, structural characterization, luminescence stability tests, and cytotoxicity assays of the CDs (PDF)

AUTHOR INFORMATION

Corresponding Author

*E-mail: hmxiong@fudan.edu.cn.

Notes

The authors declare no competing financial interest.

ACKNOWLEDGMENTS

This work was supported by the National Major Basic Research Program of China (2013CB934101), the National Natural Science Foundation of China (21271045), and NCET-11-0115.

REFERENCES

(1) Baker, S. N.; Baker, G. A. Luminescent Carbon Nanodots: Emergent Nanolights. *Angew. Chem., Int. Ed.* **2010**, *49*, 6726–6744.
(2) Lim, S. Y.; Shen, W.; Gao, Z. Carbon Quantum Dots and Their Applications. *Chem. Soc. Rev.* **2015**, *44*, 362–381.
(3) Hola, K.; Zhang, Y.; Wang, Y.; Giannelis, E. P.; Zboril, R.; Rogach, A. L. Carbon Dots—Emerging Light Emitters for Bioimaging, Cancer Therapy and Optoelectronics. *Nano Today* **2014**, *9*, 590–603.
(4) Li, H. T.; Kang, Z. H.; Liu, Y.; Lee, S. T. Carbon Nanodots: Synthesis, Properties and Applications. *J. Mater. Chem.* **2012**, *22*, 24230–24253.
(5) Miao, P.; Han, K.; Tang, Y.; Wang, B.; Lin, T.; Cheng, W. Recent Advances in Carbon Nanodots: Synthesis, Properties and Biomedical Applications. *Nanoscale* **2015**, *7*, 1586–1595.
(6) Zheng, X. T.; Ananthanarayanan, A.; Luo, K. Q.; Chen, P. Glowing Graphene Quantum Dots and Carbon Dots: Properties, Syntheses, and Biological Applications. *Small* **2015**, *11*, 1620–1636.
(7) Sun, Y. P.; Zhou, B.; Lin, Y.; Wang, W.; Fernando, K. A.; Pathak, P.; Meziani, M. J.; Harruff, B. A.; Wang, X.; Wang, H.; et al. Quantum-Sized Carbon Dots for Bright and Colorful Photoluminescence. *J. Am. Chem. Soc.* **2006**, *128*, 7756–7757.
(8) Li, W.; Zhang, Z.; Kong, B.; Feng, S.; Wang, J.; Wang, L.; Yang, J.; Zhang, F.; Wu, P.; Zhao, D. Simple and Green Synthesis of Nitrogen-Doped Photoluminescent Carbonaceous Nanospheres for Bioimaging. *Angew. Chem., Int. Ed.* **2013**, *52*, 8151–8155.
(9) Xu, Y.; Wu, M.; Liu, Y.; Feng, X. Z.; Yin, X. B.; He, X. W.; Zhang, Y. K. Nitrogen-Doped Carbon Dots: A Facile and General Preparation Method, Photoluminescence Investigation, and Imaging Applications. *Chem. - Eur. J.* **2013**, *19*, 2276–2283.
(10) Ruan, S.; Qian, J.; Shen, S.; Zhu, J.; Jiang, X.; He, Q.; Gao, H. A Simple One-Step Method to Prepare Fluorescent Carbon Dots and Their Potential Application in Non-Invasive Glioma Imaging. *Nanoscale* **2014**, *6*, 10040–10047.

DOI: 10.1021/acsnano.5b05406
ACS Nano 2016, 10, 484–491

(11) Vinci, J. C.; Colon, L. A. Fractionation of Carbon-Based Nanomaterials by Anion-Exchange HPLC. *Anal. Chem.* **2012**, *84*, 1178−1183.
(12) Vinci, J. C.; Ferrer, I. M.; Seedhouse, S. J.; Bourdon, A. K.; Reynard, J. M.; Foster, B. A.; Bright, F. V.; Colón, L. A. Hidden Properties of Carbon Dots Revealed After HPLC Fractionation. *J. Phys. Chem. Lett.* **2013**, *4*, 239−243.
(13) Gong, X.; Hu, Q.; Paau, M. C.; Zhang, Y.; Shuang, S.; Dong, C.; Choi, M. M. Red-Green-Blue Fluorescent Hollow Carbon Nanoparticles Isolated from Chromatographic Fractions for Cellular Imaging. *Nanoscale* **2014**, *6*, 8162−8170.
(14) Hu, Q.; Paau, M. C.; Choi, M. M. F.; Zhang, Y.; Gong, X.; Zhang, L.; Liu, Y.; Yao, J. Better Understanding of Carbon Nanoparticles via High-Performance Liquid Chromatography-Fluorescence Detection and Mass Spectrometry. *Electrophoresis* **2014**, *35*, 2454−2462.
(15) Gong, X.; Hu, Q.; Chin Paau, M.; Zhang, Y.; Zhang, L.; Shuang, S.; Dong, C.; Choi, M. M. F. High-Performance Liquid Chromatographic and Mass Spectrometric Analysis of Fluorescent Carbon Nanodots. *Talanta* **2014**, *129*, 529−538.
(16) Liu, H.; Ye, T.; Mao, C. Fluorescent Carbon Nanoparticles Derived from Candle Soot. *Angew. Chem., Int. Ed.* **2007**, *46*, 6473−6475.
(17) Tao, H.; Yang, K.; Ma, Z.; Wan, J.; Zhang, Y.; Kang, Z.; Liu, Z. *In Vivo* NIR Fluorescence Imaging, Biodistribution, and Toxicology of Photoluminescent Carbon Dots Produced from Carbon Nanotubes and Graphite. *Small* **2012**, *8*, 281−290.
(18) Ko, H. Y.; Chang, Y. W.; Paramasivam, G.; Jeong, M. S.; Cho, S.; Kim, S. *In Vivo* Imaging of Tumour Bearing Near-Infrared Fluorescence-Emitting Carbon Nanodots Derived from Tire Soot. *Chem. Commun.* **2013**, *49*, 10290−10292.
(19) Hu, S.; Trinchi, A.; Atkin, P.; Cole, I. Tunable Photoluminescence Across the Entire Visible Spectrum from Carbon Dots Excited by White Light. *Angew. Chem., Int. Ed.* **2015**, *54*, 2970−2974.
(20) Fu, M.; Ehrat, F.; Wang, Y.; Milowska, K. Z.; Reckmeier, C.; Rogach, A. L.; Stolarczyk, J. K.; Urban, A. S.; Feldmann, J. Carbon Dots: A Unique Fluorescent Cocktail of Polycyclic Aromatic Hydrocarbons. *Nano Lett.* **2015**, *15*, 6030−6035.
(21) Lu, Y.; Zhang, L.; Lin, H. The Use of a Microreactor for Rapid Screening of the Reaction Conditions and Investigation of the Photoluminescence Mechanism of Carbon Dots. *Chem. - Eur. J.* **2014**, *20*, 4246−4250.
(22) Nie, H.; Li, M.; Li, Q.; Liang, S.; Tan, Y.; Sheng, L.; Shi, W.; Zhang, S. X.-A. Carbon Dots with Continuously Tunable Full-Color Emission and Their Application in Ratiometric pH Sensing. *Chem. Mater.* **2014**, *26*, 3104−3112.
(23) Zhai, X.; Zhang, P.; Liu, C.; Bai, T.; Li, W.; Dai, L.; Liu, W. Highly Luminescent Carbon Nanodots by Microwave-Assisted Pyrolysis. *Chem. Commun.* **2012**, *48*, 7955−7957.
(24) Jiang, K.; Sun, S.; Zhang, L.; Lu, Y.; Wu, A.; Cai, C.; Lin, H. Red, Green, and Blue Luminescence by Carbon Dots: Full-Color Emission Tuning and Multicolor Cellular Imaging. *Angew. Chem., Int. Ed.* **2015**, *54*, 5360−5363.
(25) Bao, L.; Liu, C.; Zhang, Z. L.; Pang, D. W. Photoluminescence-Tunable Carbon Nanodots: Surface-State Energy-Gap Tuning. *Adv. Mater.* **2015**, *27*, 1663−1667.
(26) Ding, H.; Wei, J. S.; Xiong, H. M. Nitrogen and Sulfur Co-doped Carbon Dots with Strong Blue Luminescence. *Nanoscale* **2014**, *6*, 13817−13823.
(27) Krysmann, M. J.; Kelarakis, A.; Dallas, P.; Giannelis, E. P. Formation Mechanism of Carbogenic Nanoparticles with Dual Photoluminescence Emission. *J. Am. Chem. Soc.* **2012**, *134*, 747−750.
(28) Zhu, S.; Song, Y.; Zhao, X.; Shao, J.; Zhang, J.; Yang, B. The Photoluminescence Mechanism in Carbon Dots (Graphene Quantum dots, Carbon Nanodots, and Polymer Dots): Current State and Future Perspective. *Nano Res.* **2015**, *8*, 355−381.
(29) Zhu, S.; Meng, Q.; Wang, L.; Zhang, J.; Song, Y.; Jin, H.; Zhang, K.; Sun, H.; Wang, H.; Yang, B. Highly Photoluminescent Carbon Dots for Multicolor Patterning, Sensors, and Bioimaging. *Angew. Chem., Int. Ed.* **2013**, *52*, 3953−3957.
(30) Dong, Y.; Pang, H.; Yang, H. B.; Guo, C.; Shao, J.; Chi, Y.; Li, C. M.; Yu, T. Carbon-Based Dots Co-doped with Nitrogen and Sulfur for High Quantum Yield and Excitation-Independent Emission. *Angew. Chem., Int. Ed.* **2013**, *52*, 7800−7804.
(31) Qu, S.; Wang, X.; Lu, Q.; Liu, X.; Wang, L. A Biocompatible Fluorescent Ink Based on Water-Soluble Luminescent Carbon Nanodots. *Angew. Chem., Int. Ed.* **2012**, *51*, 12215−12218.
(32) Ding, H.; Xiong, H.-M. Exploring the Blue Luminescence Origin of Nitrogen-doped Carbon Dots by Controlling the Water Amount in Synthesis. *RSC Adv.* **2015**, *5*, 66528−66533.
(33) Bao, L.; Zhang, Z. L.; Tian, Z. Q.; Zhang, L.; Liu, C.; Lin, Y.; Qi, B.; Pang, D. W. Electrochemical Tuning of Luminescent Carbon Nanodots: From Preparation to Luminescence Mechanism. *Adv. Mater.* **2011**, *23*, 5801−5806.
(34) Hu, C.; Yu, C.; Li, M.; Wang, X.; Yang, J.; Zhao, Z.; Eychmuller, A.; Sun, Y. P.; Qiu, J. Chemically Tailoring Coal to Fluorescent Carbon Dots with Tuned Size and Their Capacity for Cu(II) Detection. *Small* **2014**, *10*, 4926−4933.
(35) Zhu, S.; Shao, J.; Song, Y.; Zhao, X.; Du, J.; Wang, L.; Wang, H.; Zhang, K.; Zhang, J.; Yang, B. Investigating the Surface State of Graphene Quantum Dots. *Nanoscale* **2015**, *7*, 7927−7933.
(36) Strauss, V.; Margraf, J. T.; Dolle, C.; Butz, B.; Nacken, T. J.; Walter, J.; Bauer, W.; Peukert, W.; Spiecker, E.; Clark, T.; et al. Carbon Nanodots: Toward a Comprehensive Understanding of Their Photoluminescence. *J. Am. Chem. Soc.* **2014**, *136*, 17308−17316.
(37) Tang, L.; Ji, R.; Li, X.; Bai, G.; Liu, C. P.; Hao, J.; Lin, J.; Jiang, H.; Teng, K. S.; Yang, Z.; et al. Deep Ultraviolet to Near-Infrared Emission and Photoresponse in Layered N-Doped Graphene Quantum Dots. *ACS Nano* **2014**, *8*, 6312−6320.
(38) Qu, D.; Sun, Z.; Zheng, M.; Li, J.; Zhang, Y.; Zhang, G.; Zhao, H.; Liu, X.; Xie, Z. Three Colors Emission from S,N Co-doped Graphene Quantum Dots for Visible Light H_2 Production and Bioimaging. *Adv. Opt. Mater.* **2015**, *3*, 360−367.
(39) Mewada, A.; Pandey, S.; Thakur, M.; Jadhav, D.; Sharon, M. Swarming Carbon Dots for Folic Acid Mediated Delivery of Doxorubicin and Biological Imaging. *J. Mater. Chem. B* **2014**, *2*, 698.
(40) Chua, C. K.; Sofer, Z.; Šimek, P.; Jankovský, O.; Klímová, K.; Bakardjieva, S.; Hrdličková Kučková, Š.; Pumera, M. Synthesis of Strongly Fluorescent Graphene Quantum Dots by Cage-Opening Buckminsterfullerene. *ACS Nano* **2015**, *9*, 2548−2555.
(41) Peng, J.; Gao, W.; Gupta, B. K.; Liu, Z.; Romero-Aburto, R.; Ge, L.; Song, L.; Alemany, L. B.; Zhan, X.; Gao, G.; et al. Graphene Quantum Dots Derived from Carbon Fibers. *Nano Lett.* **2012**, *12*, 844−849.
(42) Zhou, J.; Yang, Y.; Zhang, C. Y. A Low-temperature Solid-phase Method to Synthesize Highly Fluorescent Carbon Nitride Dots with Tunable Emission. *Chem. Commun.* **2013**, *49*, 8605−8607.
(43) Wang, B. B.; Cheng, Q. J.; Wang, L. H.; Zheng, K.; Ostrikov, K. The Effect of Temperature on the Mechanism of Photoluminescence from Plasma-Nucleated, Nitrogenated Carbon Nanotips. *Carbon* **2012**, *50*, 3561−3571.
(44) Yang, P.; Zhao, J.; Zhang, L.; Li, L.; Zhu, Z. Intramolecular Hydrogen Bonds Quench Photoluminescence and Enhance Photocatalytic Activity of Carbon Nanodots. *Chem. - Eur. J.* **2015**, *21*, 8561−8568.
(45) Wang, C.; Xu, Z.; Cheng, H.; Lin, H.; Humphrey, M. G.; Zhang, C. A Hydrothermal Route to Water-Stable Luminescent Carbon Dots as Nanosensors for pH and Temperature. *Carbon* **2015**, *82*, 87−95.
(46) Qu, D.; Zheng, M.; Zhang, L.; Zhao, H.; Xie, Z.; Jing, X.; Haddad, R. E.; Fan, H.; Sun, Z. Formation Mechanism and Optimization of Highly Luminescent N-Doped Graphene Quantum Dots. *Sci. Rep.* **2014**, *4*, 5294.
(47) Wang, L.; Zhu, S. J.; Wang, H. Y.; Qu, S. N.; Zhang, Y. L.; Zhang, J. H.; Chen, Q. D.; Xu, H. L.; Han, W.; Yang, B.; et al. Common Origin of Green Luminescence in Carbon Nanodots and Graphene Quantum Dots. *ACS Nano* **2014**, *8*, 2541−2547.

DOI: 10.1021/acsnano.5b05406
ACS Nano 2016, 10, 484−491

(48) Zhu, S.; Zhang, J.; Tang, S.; Qiao, C.; Wang, L.; Wang, H.; Liu, X.; Li, B.; Li, Y.; Yu, W.; et al. Surface Chemistry Routes to Modulate the Photoluminescence of Graphene Quantum Dots: From Fluorescence Mechanism to Up-Conversion Bioimaging Applications. *Adv. Funct. Mater.* **2012**, *22*, 4732−4740.
(49) Lu, S.; Zhao, X.; Zhu, S.; Song, Y.; Yang, B. Novel Cookie-with-Chocolate Carbon Dots Displaying Extremely Acidophilic High Luminescence. *Nanoscale* **2014**, *6*, 13939−13944.
(50) Chien, C. T.; Li, S. S.; Lai, W. J.; Yeh, Y. C.; Chen, H. A.; Chen, I. S.; Chen, L. C.; Chen, K. H.; Nemoto, T.; Isoda, S.; et al. Tunable Photoluminescence from Graphene Oxide. *Angew. Chem., Int. Ed.* **2012**, *51*, 6662−6666.
(51) Ghosh, S.; Chizhik, A. M.; Karedla, N.; Dekaliuk, M. O.; Gregor, I.; Schuhmann, H.; Seibt, M.; Bodensiek, K.; Schaap, I. A.; Schulz, O.; et al. Photoluminescence of Carbon Nanodots: Dipole Emission Centers and Electron-Phonon Coupling. *Nano Lett.* **2014**, *14*, 5656−5661.
(52) Song, Y.; Zhu, S.; Xiang, S.; Zhao, X.; Zhang, J.; Zhang, H.; Fu, Y.; Yang, B. Investigation into the Fluorescence Quenching Behaviors and Applications of Carbon Dots. *Nanoscale* **2014**, *6*, 4676−4682.
(53) Ye, R.; Xiang, C.; Lin, J.; Peng, Z.; Huang, K.; Yan, Z.; Cook, N. P.; Samuel, E. L.; Hwang, C. C.; Ruan, G.; et al. Coal as an Abundant Source of Graphene Quantum Dots. *Nat. Commun.* **2013**, *4*, 2943.
(54) Wu, Z. L.; Gao, M. X.; Wang, T. T.; Wan, X. Y.; Zheng, L. L.; Huang, C. Z. A General Quantitative pH Sensor Developed with Dicyandiamide N-Doped High Quantum Yield Graphene Quantum Dots. *Nanoscale* **2014**, *6*, 3868−3874.
(55) Song, Y. B.; Zhu, S. J.; Yang, B. Bioimaging Based on Fluorescent Carbon Dots. *RSC Adv.* **2014**, *4*, 27184−27200.
(56) Nurunnabi, M.; Khatun, Z.; Huh, K. M.; Park, S. Y.; Lee, D. Y.; Cho, K. J.; Lee, Y.-k *In Vivo* Biodistribution and Toxicology of Carboxylated Graphene Quantum Dots. *ACS Nano* **2013**, *7*, 6858−6867.
(57) Yang, S. T.; Cao, L.; Luo, P. G.; Lu, F.; Wang, X.; Wang, H.; Meziani, M. J.; Liu, Y.; Qi, G.; Sun, Y. P. Carbon Dots for Optical Imaging *in Vivo*. *J. Am. Chem. Soc.* **2009**, *131*, 11308−11309.

DOI: 10.1021/acsnano.5b05406
ACS Nano 2016, 10, 484−491